(Received 19 June 2025, Accepted 25 July 2025, Scheduled 4 August 2025)

A Defected Ground Structure Design for Reducing Coupling in Dual-Band MIMO Antennas

Junhao Xu[1, 2] and Yafei Wang[1, 2, *]

[1] *Key Laboratory of Information and Communication Systems, Ministry of Information Industry, Beijing Information Science and Technology University, Beijing 100101, China*
[2] *Key Laboratory of Modern Measurement & Control Technology, Ministry of Education Beijing Information Science and Technology University, Beijing 100101, China*

ABSTRACT: This paper presents a compact multiple-input multiple-output (MIMO) microstrip antenna system covering the 2.4 GHz and 5 GHz wireless local area network (WLAN) bands. By etching rectangular slots on the microstrip patch and adjusting the dimensions of both the antenna and rectangular slots, the antenna system can radiate at the operating frequencies of 2.44 GHz and 5.3 GHz simultaneously. To achieve high port isolation across the two distinct WLAN bands, a "WM"-shaped defected ground structure (DGS) is etched on the ground plane to reduce mutual coupling in the 2.44/5.3 GHz frequency bands. Simulation results demonstrate that within the frequency ranges of 2.41–2.49 GHz and 5.22–5.39 GHz, the isolation of the two dual-band antenna systems achieves maximum coupling suppression of 26.7 dB and 14 dB, respectively. This DGS can serve as a potential solution for decoupling in WLAN MIMO antennas.

1. INTRODUCTION

With the development of wireless communication technology entering a new era, the demand for reliable data transmission rates is growing rapidly. On the other hand, due to the sharp increase in the number of users, the available wireless communication spectrum is facing the limitation of high traffic. In recent years, MIMO technology has attracted great attention from researchers because this technology can provide higher data rates, better reliability and spectral efficiency under the same bandwidth and power level, and has a stronger ability to overcome multipath fading in the scattering environment [1]. In order to realize the MIMO antenna system, it is necessary to place multiple antennas in a specific area. Therefore, signal interference will occur between antennas, especially in the case of limited space [2, 3]. Therefore, decoupling multiple compactly placed antennas in MIMO systems is a challenge. Many compact single-band wireless local area network (WLAN) antennas have been studied [4, 5]. However, due to the rapid development of wireless services, the demand for multi-band antennas has become urgent. For example, the wireless local area network standard IEEE 802.11ax covers the 2.4 GHz and 5 GHz frequency bands, so a dual-band antenna that can cover both frequency bands at the same time is required. For MIMO WLAN, how to achieve high isolation between multi-band antenna elements has become a critical issue.

In the past few years, much work has been devoted to improving the isolation of single-band antennas [6–9]. In addition, several methods have been proposed to reduce the mutual coupling between multi-band antennas. Decoupling networks have been widely studied and used to improve the mutual coupling of dual-band antennas [10–12]. In [10], a decoupling network is proposed based on parallel-line coupling elements for dual-band antenna decoupling. In [11], a dual-frequency coupled resonator decoupling network is proposed, which consists of a pair of dual-frequency open-loop square resonators, thereby improving the mutual coupling between antennas. Although decoupling networks have demonstrated good decoupling effects in many studies, they also increase the complexity and loss of the antenna system. Other effective methods for reducing mutual coupling in dual-band antennas include metamaterials [13, 14], resonant elements [15–17], and electromagnetic bandgap [18]. In [13], the metasurface coating consists of paired slotted lines with two different lengths, which can effectively decouple adjacent dual-band antennas. However, the metasurface decoupling method suffers from the problems of a bulky structure and time-consuming optimization. In some studies, parasitic elements such as planar spirals [16], parasitic resonators [19], and metal strips [20] are introduced between/around antenna elements or into the antenna elements themselves. Additionally, DGS is also an excellent solution for reducing mutual coupling in dual-band antennas [21–24]. High isolation between ports can be achieved by etching slots in the ground plane.

All the above-mentioned works have achieved the reduction of mutual coupling between dual-band antennas, but they usually suffer from the problems of bulky decoupling structures, time-consuming optimization, and high complexity and high loss of the antenna system caused by the introduction of decoupling structures. Therefore, achieving high isolation between dual-band antenna ports in an intuitive manner remains a huge challenge.

* Corresponding author: Yafei Wang (wangyafei@bistu.edu.cn).

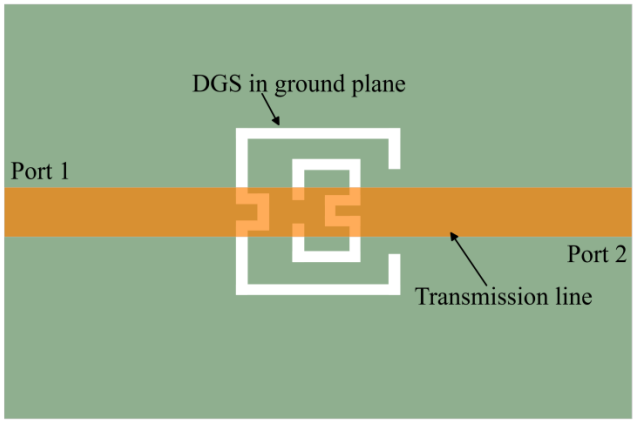

FIGURE 1. Microstrip line model loaded with "WM"-shaped DGS.

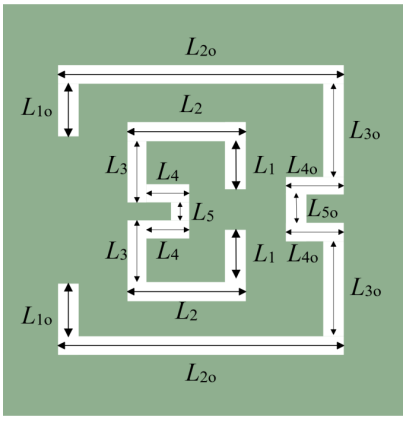

FIGURE 2. Planar structure of the "WM"-shaped DGS.

This paper presents a dual-band MIMO microstrip antenna system for WLAN applications. The designed antenna operates at both 2.4 GHz and 5 GHz bands. Dual-band characteristics are achieved by etching a slot on the microstrip antenna patch. Subsequently, by etching a "WM"-shaped DGS on the ground plane, decoupling of the antenna is successively realized in both the low and high frequency bands. The designed dual-band MIMO antenna has been fabricated and tested. The proposed design is compact and exhibits dual-band performance, demonstrating its potential as a candidate for access point applications.

The structure of this paper is organized as follows. Section 2 introduces and analyzes the characteristics of the "WM"-shaped DGS. Section 3 presents the design of the dual-band microstrip antenna loaded with this DGS. Section 4 discusses the simulation and measurement results of the microstrip antenna. Conclusions are made in Section 5.

2. ``WM"-SHAPED DGS AND CHARACTERISTIC ANALYSIS

To analyze the characteristics of the "WM"-shaped DGS, a microstrip line model loaded with the DGS is established as shown in Fig. 1. A microstrip transmission line with a characteristic impedance of 50 Ω is placed on the upper layer of the dielectric substrate, which is made of Rogers 5880 with a relative permittivity of 2.2 and a thickness $h = 1.5$ mm. The "WM"-shaped DGS is etched on the metal plate of the ground plane of the dielectric substrate. The frequency range of the high frequency structure simulator (HFSS) is set to $2 \sim 6$ GHz, and the transmission loss coefficient S_{21} between the two ports is examined using HFSS.

The planar structure of the DGS is illustrated in Fig. 2, where the key parameters affecting the filtering performance are L_1, L_2, L_4, L_5, L_{2o}, L_{3o}, and L_{5o}. The following section will analyze the impact of each parameter on the DGS filtering characteristics in detail. It should be noted that the parameter analysis presented here aims to investigate the individual influence of each parameter on the filtering performance. The results should not be considered as the final dimensions for the DGS integrated into the MIMO antenna but rather as initial values. Since the DGS in the antenna is arranged periodically, the final dimensions require further fine-tuning after being incorporated into the microstrip antenna to determine the optimal parameter values.

2.1. Influence of Parameters L_1, L_2, L_4, and L_{5o}

Using the microstrip line model loaded with the DGS, simulations were conducted to analyze the filtering characteristics under varying lengths of parameters L_1, L_2, L_4, and L_{5o} while keeping other parameters constant. The results are presented in Figs. 3, 4, 5, and 6, where different curves correspond to different lengths of L_1, L_2, L_4, and L_{5o}. It can be observed that as the lengths of L_1, L_2, L_4, and L_{5o} increase, the high-frequency resonance points shift towards the lower frequency band. Moreover, parameters L_1 and L_2 exert a stronger influence on the high-frequency resonance points of the DGS filter than parameters L_4 and L_{5o}.

2.2. Influence of Parameters L_5, L_{2o}, and L_{3o}

Figures 7 and 8 illustrate the filtering characteristics of the DGS filter under different lengths of L_5 and L_{2o}. As shown in the figures, the low-frequency resonance points shift towards higher frequencies as the parameters L_5 and L_{2o} decrease. Fig. 9 depicts the filtering characteristics of the DGS filter under different lengths of L_{3o}. It can be observed that the low-frequency resonance points shift towards higher frequencies as the parameter L_{3o} increases, which is opposite to the effect of L_5 and L_{2o} on the filtering characteristics of the DGS. Compared with the influence of L_1 and L_2 on the high-frequency resonance points of the DGS filter, the influence of L_5, L_{2o}, and L_{3o} on the low-frequency resonance points is relatively weaker.

3. ``WM"-SHAPED DGS DESIGN FOR REDUCING ANTENNA COUPLING

3.1. Design of Dual-Band Microstrip Antenna Array without Decoupling Structure

The proposed WLAN MIMO patch antenna is shown in Fig. 10. The dielectric substrate is made of F4B with a dielectric constant of 2.2 and a thickness $h = 3$ mm. Both the dielectric

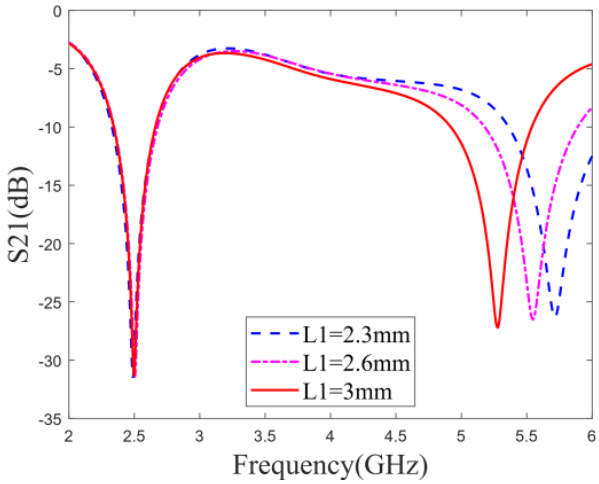

FIGURE 3. Microstrip line frequency response characteristics trend with parameter L_1.

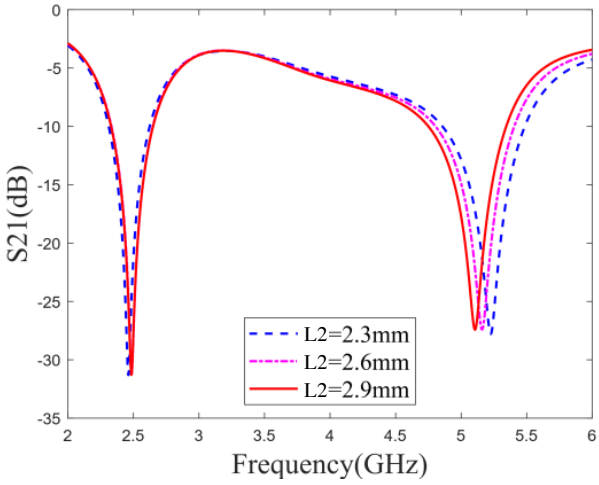

FIGURE 4. Microstrip line frequency response characteristics trend with parameter L_2.

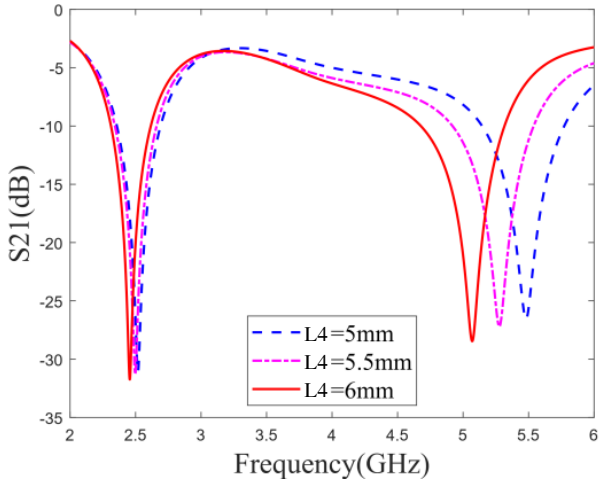

FIGURE 5. Microstrip line frequency response characteristics trend with parameter L_4.

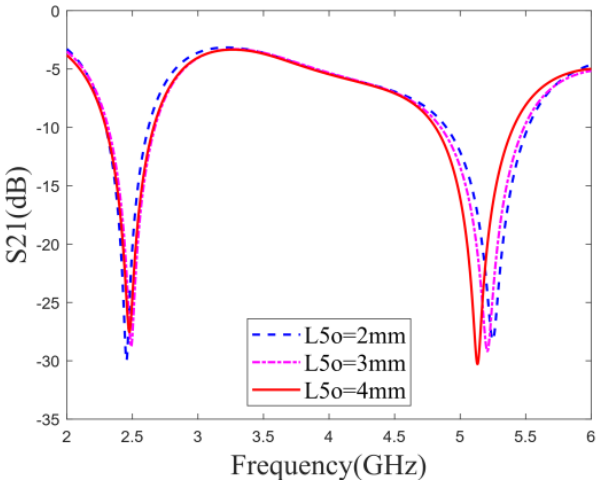

FIGURE 6. Microstrip line frequency response characteristics trend with parameter L_{5o}.

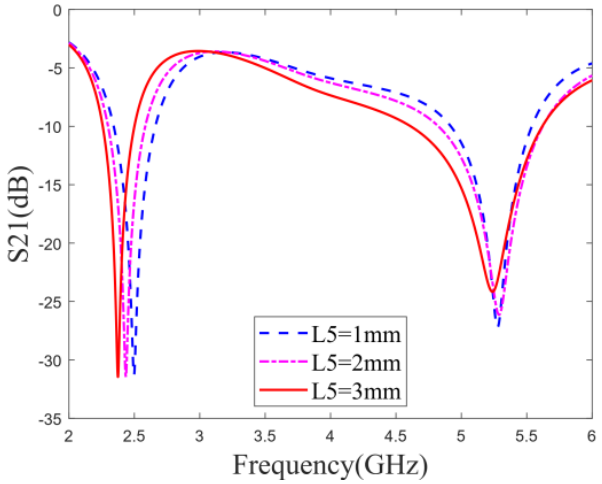

FIGURE 7. Microstrip line frequency response characteristics trend with parameter L_5.

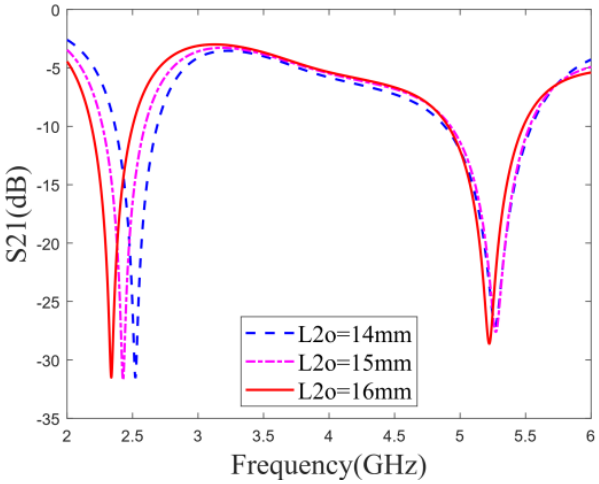

FIGURE 8. Microstrip line frequency response characteristics trend with parameter L_{2o}.

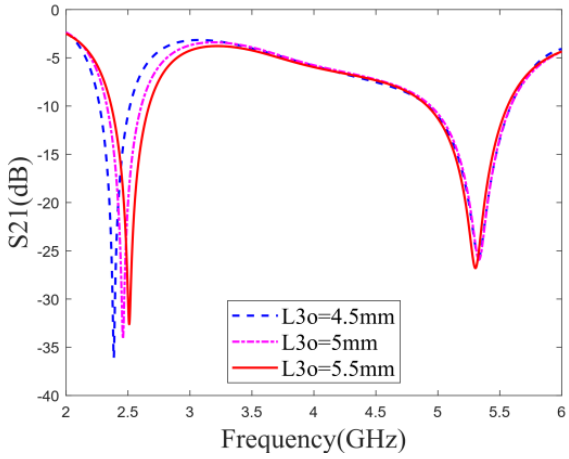

FIGURE 9. Microstrip line frequency response characteristics trend with parameter L_{3o}.

substrate and ground plane have dimensions of $W_g \times L_g$; the patch has dimensions of $W \times L$. The antenna is designed to operate in two frequency bands by controlling the dimensions of the patch, and a rectangular slot etched on the patch is used for fine-tuning the dual-frequency characteristics, with the slot dimensions being $G_w \times G_l$. The antenna adopts a coaxial feeding method, where the horizontal distance from the feeding center to the center of the rectangular patch is L_f, and the vertical distance is X_f. The inner core of the feed has a size $R = 0.7\,\text{mm}$, providing a $50\,\Omega$ matched impedance. The designed antenna is specified to operate at center frequencies of 2.44 GHz and 5.3 GHz, respectively; the antenna array spacing is S (approximately $0.16\lambda_0$, where λ_0 is the free-space wavelength at 2.44 GHz). Fig. 11 presents the parametric study on the patch width W, and the results show that the upper resonant frequency can be easily adjusted by changing the patch width. Fig. 12 describes the parametric study on the rectangular slot length G_l, indicating that the upper/lower resonant frequencies can be finely adjusted by varying the length of the rectangular slot.

3.2. Proposed Antenna Array with Decoupling Structure

To implement a MIMO antenna system, multiple antennas must be placed within a specific spatial volume, which inevitably reduces the inter-element spacing. Such reduced spacing often leads to strong mutual coupling between antennas. To mitigate this coupling effect, the "WM"-shaped DGS designed in the previous section is integrated into the ground plane of the microstrip antenna array. The configuration of the microstrip antenna array loaded with the "WM"-shaped DGS is illustrated in Fig. 13.

The distance from the centroid of the DGS located at the lower position to the center of the ground plane is denoted as m_1, while the distance from the centroid of the DGS at the upper position to the ground plane center is m_2. Using HFSS for parametric sweep analysis of the antenna structure, the optimal dimensions of the antenna and "WM"-shaped DGS are summarized in Table 1.

TABLE 1. Antenna arrays and "WM"-shaped DGS dimensions.

	W	L	W_g	L_g	L_f	X_f	G_l
Parameters (in mm)	41.1	37	65	112	17	25	4
	L_{1o}	L_{2o}	L_{3o}	L_{4o}	L_{5o}	g	G_w
	3.7	12.9	3.8	5.2	2	0.9	4
	L_1	L_2	L_3	L_4	L_5	m_1	m_2
	0.1	7.1	2.9	2.7	1.2	6.5	14

4. EXPERIMENTAL AND MEASUREMENT RESULTS

To validate the effectiveness of the "WM"-shaped DGS in suppressing the mutual coupling between microstrip antenna elements, this section employs HFSS software to simulate the proposed microstrip antenna array integrated with the "WM"-shaped DGS. The dimensions of both the "WM"-shaped DGS and microstrip antennas are provided in Table 1. The simulation frequency range is set from 2 GHz to 6 GHz, and the results include S-parameters, Envelope Correlation Coefficient (ECC), and far-field radiation patterns.

4.1. S-Parameter

The performance of the antenna can be evaluated by S_{11} and S_{21}, where S_{11} is the reflection coefficient of the antenna port, indicating the amount of energy reflected from the antenna port; S_{21} is the coupling coefficient from the first antenna to the second antenna, which is numerically equal to the ratio of the signal power between the second antenna port and the first antenna port, and a smaller value of S_{21} indicates a lower coupling between the two antennas.

The resonant frequency of the antenna is defined as the frequency range within which the antenna meets the operational requirements and thus realizes the effective reception and transmission of the signal. For the antenna, the resonant frequency is defined as the frequency range in which the reflection coefficient S_{11} of the antenna is below -10 dB. The center frequency of the antenna is defined as the frequency corresponding to the lowest S_{11} in the resonant frequency range, and the gain and efficiency of the antenna reach the maximum values at the center frequency.

The simulation results of the S-parameters of the microstrip antenna array before and after loading the "WM"-shaped DGS are shown in Figs. 14 and 15, respectively. The results indicate that there is no significant change in the antenna's S_{11} before and after loading the DGS. Before loading the DGS, the S_{21} of the microstrip antenna is -21 dB at 2.44 GHz and -16.38 dB at 5.3 GHz. After loading the DGS, the S_{21} of the microstrip antenna becomes -47.71 dB at 2.44 GHz and -30.42 dB at 5.3 GHz. This demonstrates that loading the DGS effectively reduces the coupling between antenna arrays by 26.71 dB at 2.44 GHz and 14.04 dB at 5.3 GHz. This verifies the band-stop filtering characteristics of the designed "WM"-shaped DGS, achieves the blocking of coupling currents on the ground plane, and can effectively reduce the mutual coupling between antenna arrays.

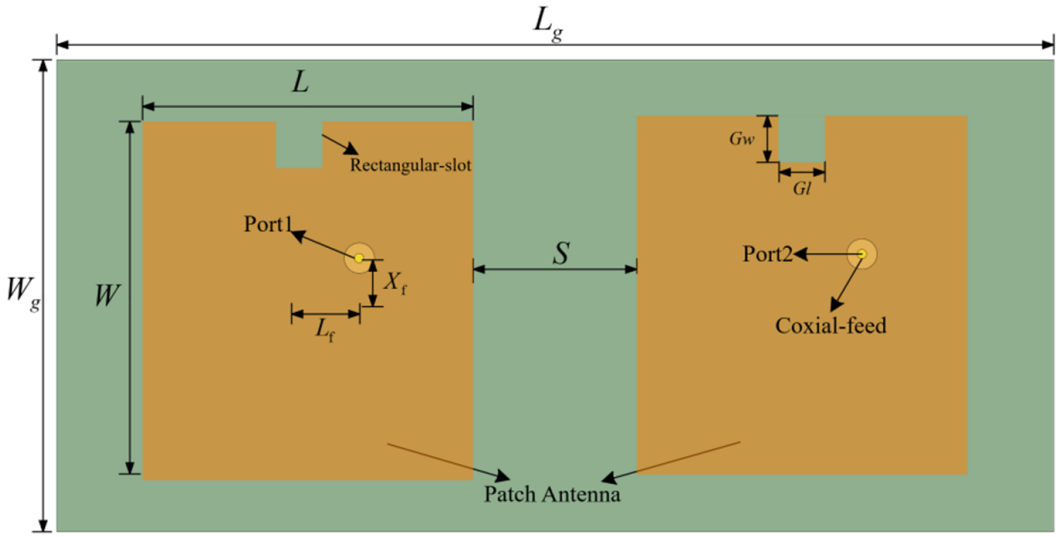

FIGURE 10. Original antenna array structure without decoupling design.

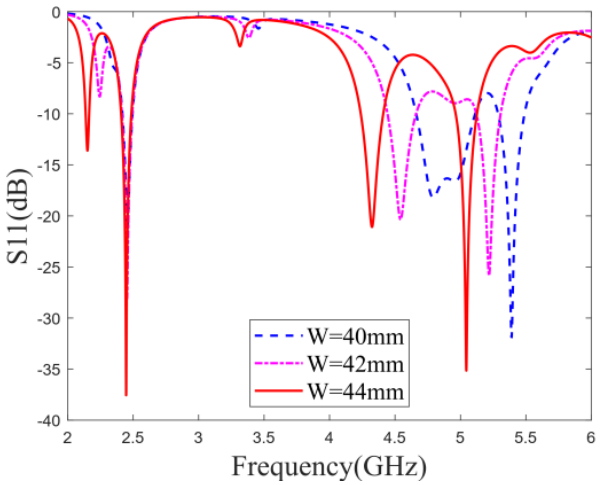

FIGURE 11. Simulated S_{11} of the proposed antenna with parameter W.

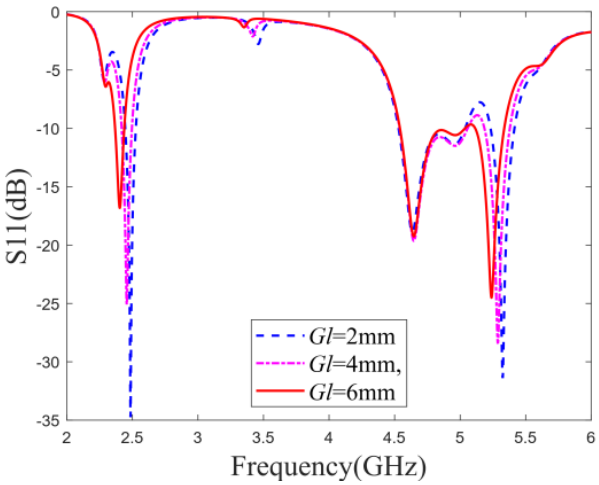

FIGURE 12. Simulated S_{11} of the proposed antenna with parameter Gl.

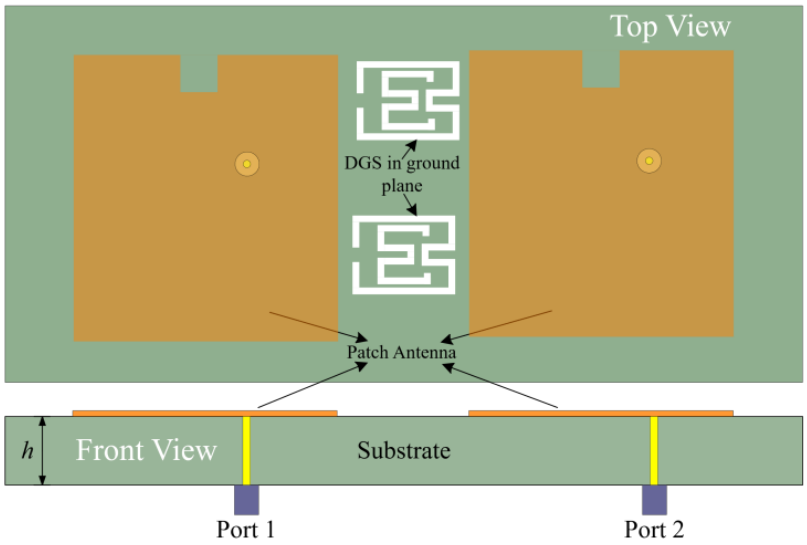

FIGURE 13. Microstrip antenna array loaded with "WM"-shaped DGS.

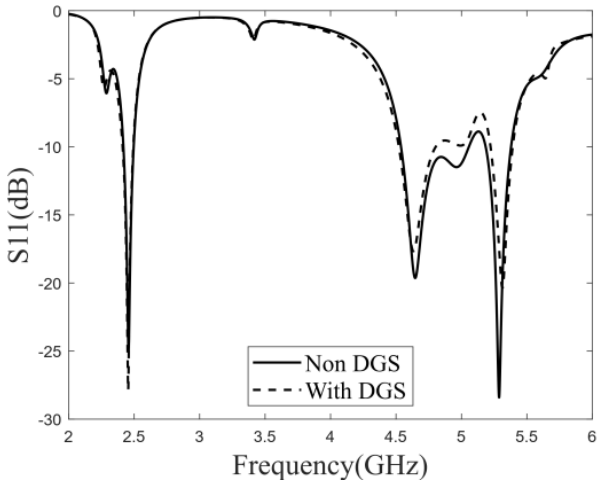

FIGURE 14. S_{11} simulation results with and without "WM"-shaped DGS.

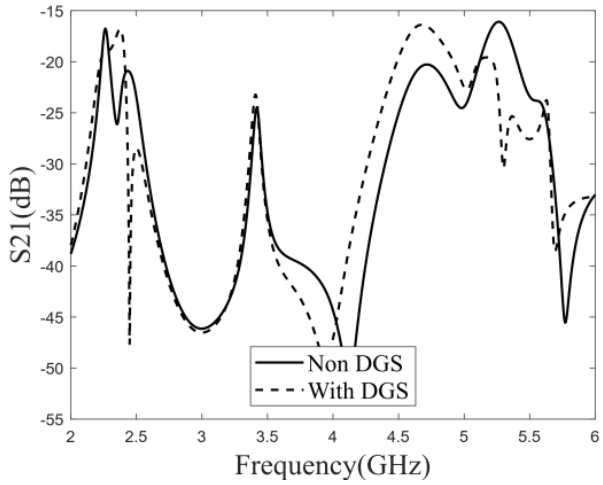

FIGURE 15. S_{21} simulation results with and without "WM"-shaped DGS.

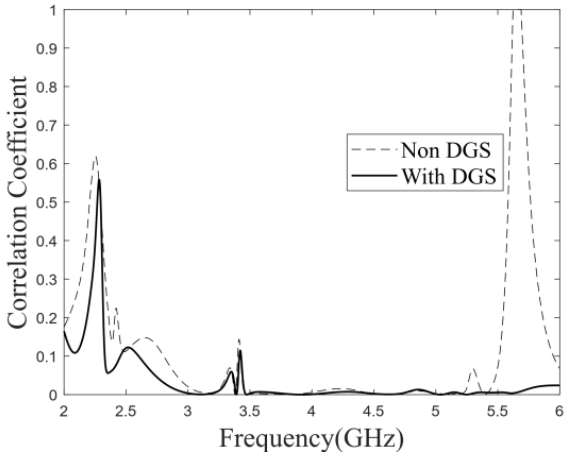

FIGURE 16. Correlation coefficients of microstrip antenna arrays with and without "WM"-shaped DGS.

4.2. Correlation Coefficient

The spatial correlation of the signal is a key factor affecting the performance of the MIMO systems. The spatial correlation of the antenna refers to the correlation characteristics between the antenna at the transmitting end and the antenna at the receiving end, which is generally expressed by the correlation coefficient. If the correlation coefficient is too large, the channel capacity of the MIMO systems will be significantly lost. In order to achieve good performance, a necessary condition is to have a low correlation between the transmitter and receiver antennas.

The correlation between the envelopes of two signals is known as the ECC, and it is calculated by Formula (1):

$$\rho_e = \frac{E\left\{\left(|x_1|^2 - E\left\{|x_1|^2\right\}\right)\left(|x_2|^2 - E\left\{|x_2|^2\right\}\right)^*\right\}}{\sqrt{E\left\{\left||x_1|^2 - E\left\{|x_1|^2\right\}\right|^2\right\} E\left\{\left||x_2|^2 - E\left\{|x_2|^2\right\}\right|^2\right\}}} \tag{1}$$

where x_1 and x_2 represent the two shunt signals, respectively, and $E\{\}$ represents the expected value of the signal. ρ_e is the ECC of the antenna.

According to HFSS, the correlation coefficients of antennas with and without loading the W-shaped DGS are shown in Fig. 16. The figure shows that the overall envelope correlation coefficient is less than 0.1, which indicates that adding this structure makes the correlation coefficient between the two antennas significantly lower, demonstrating that the loading of the structure significantly improves the isolation between the antennas.

4.3. Far-Field Radiation Pattern

The central operating frequency of the microstrip antenna array is 2.44/5.3 GHz. The radiation pattern at the central operating frequency was tested respectively. The simulation pattern of the E plane and H plane is shown in Figs. 17 and 18. In the figures, the antenna gain direction shows a directional radiation characteristic. After loading the defective ground structure, at the central frequency of 2.44/5.3 GHz, the radiation pattern shows good consistency in the forward radiation of the E plane and H plane, while the backward radiation of the antenna increases by up to 9.3 dB at most. This is because part of the energy of the antenna radiates into the free space through the defective ground structure, which indicates that there is no significant difference in the radiation pattern before and after loading the "WM"-shaped DGS, but the isolation between antenna arrays is significantly improved.

To further validate the effect of the proposed "WM"-shaped DGS on reducing the coupling between the microstrip antenna arrays, the microstrip antenna arrays loaded with the "WM"-shaped DGS were processed and measured by a vector network analyzer. The prototype of the antenna arrays was fabricated according to the parameters in Table 1, as shown in Fig. 19. Fig. 19(a) shows the top view of the antenna arrays, and Fig. 19(b) shows the bottom view of the antenna arrays.

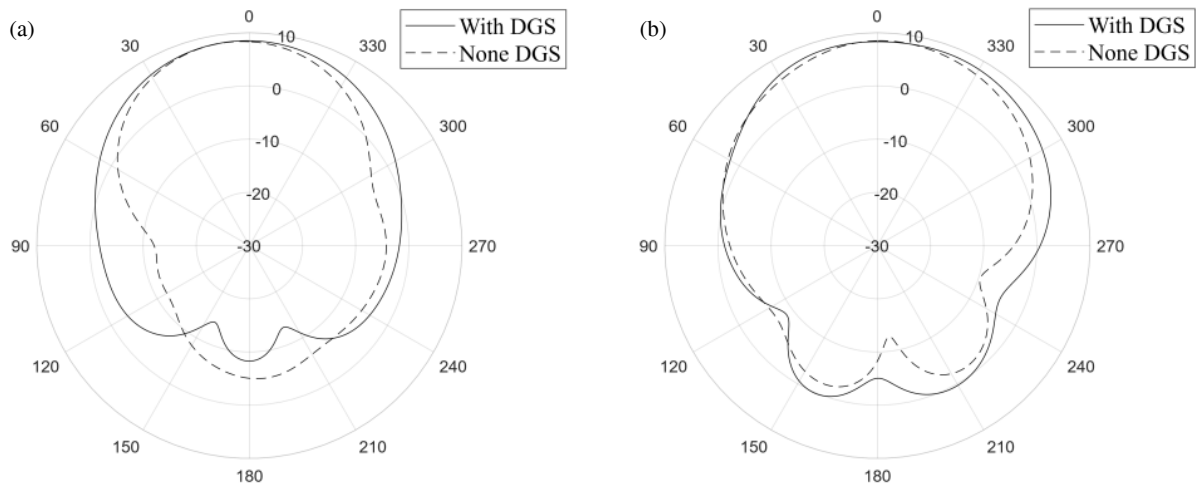

FIGURE 17. Far-field radiation pattern of microstrip antenna arrays with and without "WM"-shaped DGS (2.44 GHz). (a) E-plane. (b) H-plane.

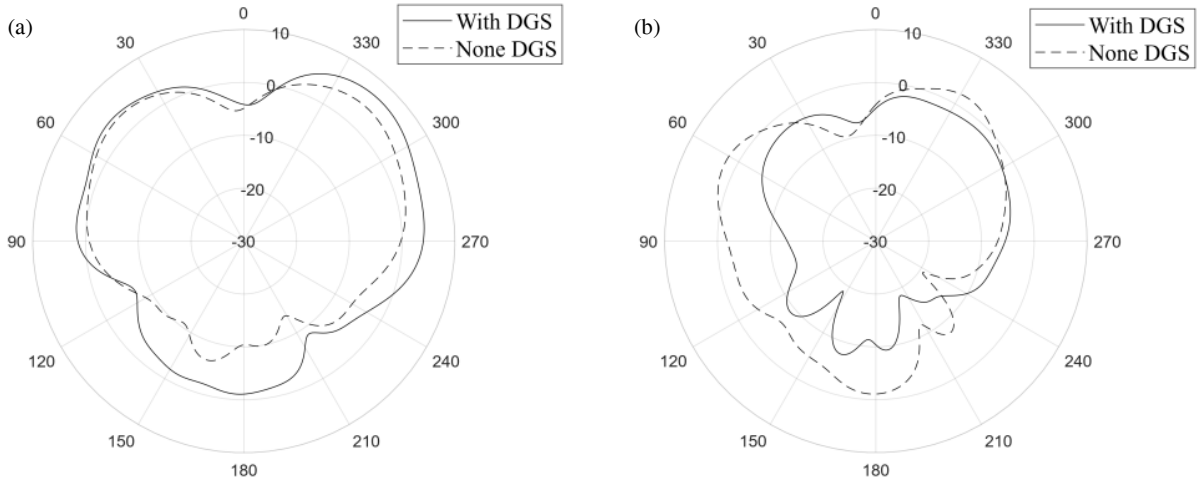

FIGURE 18. Far-field radiation pattern of microstrip antenna arrays with and without "WM"-shaped DGS (5.3 GHz). (a) E-plane. (b) H-plane.

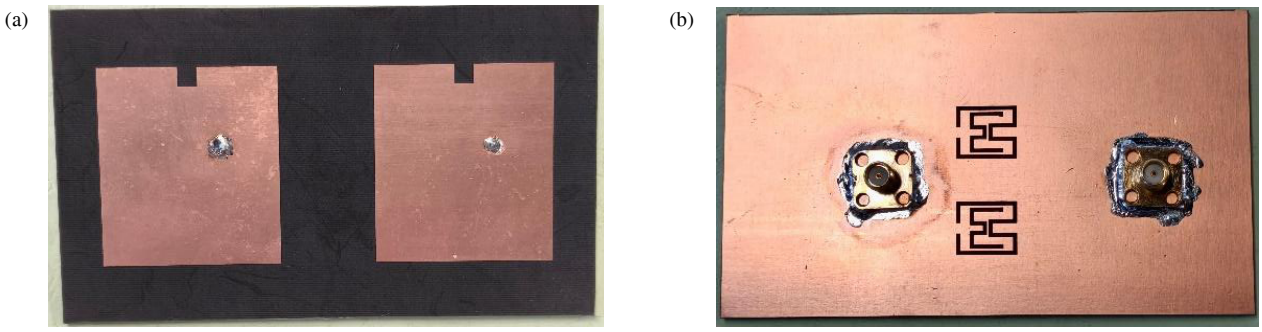

FIGURE 19. The prototype of microstrip antenna arrays with "WM"-shaped DGS. (a) Top view. (b) Bottom view.

During the measurement process, two 50 Ω SMA connectors are used to feed the antenna.

The S-parameters were measured using a vector network analyzer. Fig. 20 shows the comparison curves of the simulated and measured S_{11} and S_{21} parameters. A slight discrepancy exists between the two due to SMA connector losses and manufacturing tolerances. However, it can be observed that the measured results are in good agreement with the simulated ones obtained from HFSS. The actual measurement results indicate that the bandwidth with $S_{11} < -10$ dB at the low-frequency point is 81 MHz (2.412 $\sim$ 2.493 GHz), and the bandwidth with $S_{11} < -10$ dB at the high-frequency point is 169 MHz

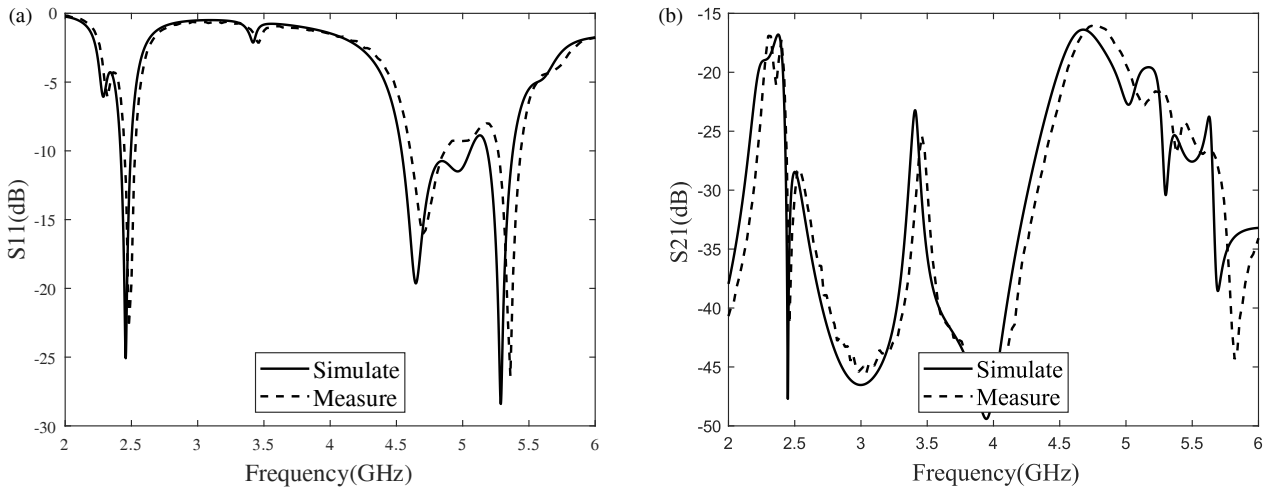

FIGURE 20. S_{11} and S_{21} simulation and measurement comparison curves. (a) S_{11} simulation and measurement comparison curves. (b) S_{21} simulation and measurement comparison curves.

TABLE 2. Comparison among the relevant works.

Ref.	Method	Frequency (GHz)	Edge-to-edge spacing (λ_0)	Isolation improvement (LB/HB) (dB)	Complexity
[12]	Decoupling network	2.35–2.5/ 5.05–5.3	0.08/0.17	13/9	medium
[15]	DGS & Resonant structure	2.4–2.483/ 5.15–5.83	0.12/0.27	12/7	High
[18]	EBG	3.42–3.6/ 4.7–5.1	0.46/0.65	25/10	High
[20]	Metal strips & walls	3.47–3.53/ 5.68–5.72	0.023/0.038	10.8/15.6	High
This work	DGS	2.41–2.49/ 5.22–5.39	0.16/0.35	26.7/14	Low

Where λ_0 is the free space wavelength at the lowest resonant frequency.

(5.222 $\sim$ 5.391 GHz). At the low-frequency range, the center frequency of S_{21} is 2.448 GHz, and the coupling value between the antenna arrays decreases from -21 dB to -41.34 dB, achieving more than 20 dB of coupling suppression. At the high-frequency range, the center frequency of S_{21} is 5.36 GHz, and the coupling value between the antenna arrays decreases from -16.38 dB to -26.8705 dB, achieving an overall coupling suppression of more than 10 dB.

Table 2 summarizes the performance of this work and other relevant works. It can be observed that although the proposed scheme requires a certain spacing, it outperforms other methods in terms of decoupling effect and structural complexity. In [12] and [20], the antenna spacing is relatively small, but the improvement in isolation in the low-frequency band and high-frequency band is not particularly significant. In [15], although the isolation between antennas is improved, the excessively high structural complexity may pose risks in practical applications. Ref. [18] has achieved remarkable results in antenna isolation; however, the issues of large spacing and high complexity remain to be improved. Therefore, it can be seen from Table 2 that the proposed DGS has the advantage of achieving a better decoupling effect within a relatively compact volume.

5. CONCLUSION

To suppress the coupling between dual-band MIMO antenna systems, this paper designs a simple and compact "WM"-shaped DGS. A microstrip line model loaded with the "WM"-shaped DGS is constructed, and the band-stop characteristics of this structure are analyzed. Subsequently, by controlling the dimensions of the patch and rectangular slot, the MIMO antenna system is made to operate at two frequency bands of 2.4 GHz and 5.3 GHz. After loading the "WM"-shaped DGS into the dual-band MIMO antenna system, the isolation between the antenna ports is reduced by 26.7 dB and 14 dB at the high-frequency and low-frequency points, respectively, and the ECC between the antennas is also reduced. A comparison with other relevant works reveals that although the proposed scheme requires a certain spacing, it outperforms other structures in both decoupling effect and structural complexity. In addition, the measured results are in good agreement with the simulated ones, which indicates that the DGS proposed in this paper can serve as a potential decoupling solution for WLAN MIMO antennas.

REFERENCES

[1] Fang, Y., Y. Liu, Y. Jia, J. Liang, and H. H. Zhang, "Reconfigurable structure reutilization low-SAR MIMO antenna for 4G/5G full-screen metal-frame smartphone operation," *IEEE Antennas and Wireless Propagation Letters*, Vol. 22, No. 5, 1219–1223, 2023.

[2] Sui, J., Y. Dou, X. Mei, and K.-L. Wu, "Self-curing decoupling technique for MIMO antenna arrays in mobile terminals," *IEEE Transactions on Antennas and Propagation*, Vol. 68, No. 2, 838–849, 2020.

[3] Hu, J., W. Zhang, Y. Li, and Z. Zhang, "Compact co-polarized PIFAs for full-duplex application based on CM/DM cancellation theory," *IEEE Transactions on Antennas and Propagation*, Vol. 69, No. 11, 7103–7110, 2021.

[4] Zhang, Y. and Y. Li, "Scalable omnidirectional dual-polarized antenna using cavity and slot-dipole hybrid structure," *IEEE Transactions on Antennas and Propagation*, Vol. 70, No. 6, 4215–4223, 2022.

[5] Li, Y., Z. Zhang, Z. Feng, and M. F. Iskander, "Design of omnidirectional dual-polarized antenna in slender and low-profile column," *IEEE Transactions on Antennas and Propagation*, Vol. 62, No. 4, 2323–2326, 2014.

[6] He, Y. and Y. Li, "Compact co-linearly polarized microstrip antenna with fence-strip resonator loading for in-band full-duplex systems," *IEEE Transactions on Antennas and Propagation*, Vol. 69, No. 11, 7125–7133, 2021.

[7] Zhang, W., J. Hu, Y. Li, and Z. Zhang, "Design of a stacked co-polarized full-duplex antenna with broadside radiation," *IEEE Transactions on Antennas and Propagation*, Vol. 69, No. 11, 7111–7118, 2021.

[8] Sun, L., Y. Li, Z. Zhang, and H. Wang, "Antenna decoupling by common and differential modes cancellation," *IEEE Transactions on Antennas and Propagation*, Vol. 69, No. 2, 672–682, 2021.

[9] Zhou, Z., Y. Li, J. Hu, Y. He, Z. Zhang, and P.-Y. Chen, "Monostatic copolarized simultaneous transmit and receive (STAR) antenna by integrated single-layer design," *IEEE Antennas and Wireless Propagation Letters*, Vol. 18, No. 3, 472–476, 2019.

[10] Xu, K.-D., H. Luyen, and N. Behdad, "A decoupling and matching network design for single-and dual-band two-element antenna arrays," *IEEE Transactions on Microwave Theory and Techniques*, Vol. 68, No. 9, 3986–3999, 2020.

[11] Zhao, L. and K.-L. Wu, "A dual-band coupled resonator decoupling network for two coupled antennas," *IEEE Transactions on Antennas and Propagation*, Vol. 63, No. 7, 2843–2850, 2015.

[12] Sui, J. and K.-L. Wu, "A general T-stub circuit for decoupling of two dual-band antennas," *IEEE Transactions on Microwave Theory and Techniques*, Vol. 65, No. 6, 2111–2121, 2017.

[13] Liu, F., J. Guo, L. Zhao, G.-L. Huang, Y. Li, and Y. Yin, "Dual-band metasurface-based decoupling method for two closely packed dual-band antennas," *IEEE Transactions on Antennas and Propagation*, Vol. 68, No. 1, 552–557, 2020.

[14] Luo, S., Y. Li, and W. Shi, "A dual-frequency antenna array with mutual coupling reduction via metamaterial structures," in *2018 IEEE International Symposium on Antennas and Propagation & USNC/URSI National Radio Science Meeting*, 1385–1386, Boston, MA, USA, 2018.

[15] Deng, J., J. Li, L. Zhao, and L. Guo, "A dual-band inverted-F MIMO antenna with enhanced isolation for WLAN applications," *IEEE Antennas and Wireless Propagation Letters*, Vol. 16, 2270–2273, 2017.

[16] Xun, J.-H., L.-F. Shi, W.-R. Liu, G.-X. Liu, and S. Chen, "Compact dual-band decoupling structure for improving mutual coupling of closely placed PIFAs," *IEEE Antennas and Wireless Propagation Letters*, Vol. 16, 1985–1989, 2017.

[17] Shen, X., F. Liu, L. Zhao, G.-L. Huang, X. Shi, Q. Huang, and A. Chen, "Decoupling of two strongly coupled dual-band antennas with reactively loaded dummy element array," *IEEE Access*, Vol. 7, 154 672–154 682, 2019.

[18] Tan, X., W. Wang, Y. Wu, Y. Liu, and A. A. Kishk, "Enhancing isolation in dual-band meander-line multiple antenna by employing split EBG structure," *IEEE Transactions on Antennas and Propagation*, Vol. 67, No. 4, 2769–2774, 2019.

[19] Liu, Q., L. Zhu, and W.-J. Lu, "Decoupling of closely spaced square patch antennas using short-circuited λ/2 microstrip line," *IEEE Antennas and Wireless Propagation Letters*, Vol. 23, No. 2, 728–732, 2024.

[20] Boukarkar, A., X. Q. Lin, Y. Jiang, L. Y. Nie, P. Mei, and Y. Q. Yu, "A miniaturized extremely close-spaced four-element dual-band MIMO antenna system with polarization and pattern diversity," *IEEE Antennas and Wireless Propagation Letters*, Vol. 17, No. 1, 134–137, 2018.

[21] Pei, T., L. Zhu, J. Wang, and W. Wu, "A low-profile decoupling structure for mutual coupling suppression in MIMO patch antenna," *IEEE Transactions on Antennas and Propagation*, Vol. 69, No. 10, 6145–6153, 2021.

[22] Wang, W., Y. Wu, W. Wang, and Y. Yang, "Isolation enhancement in dual-band monopole antenna for 5G applications," *IEEE Transactions on Circuits and Systems II: Express Briefs*, Vol. 68, No. 6, 1867–1871, 2021.

[23] Soltani, S., P. Lotfi, and R. D. Murch, "A dual-band multiport MIMO slot antenna for WLAN applications," *IEEE Antennas and Wireless Propagation Letters*, Vol. 16, 529–532, 2016.

[24] Zhang, W., Y. Li, K. Wei, and Z. Zhang, "A dual-band MIMO antenna system for 2.4/5 GHz WLAN applications," *IEEE Transactions on Antennas and Propagation*, Vol. 71, No. 7, 5749–5758, 2023.